



# Ca Doping Concentration Induced Enhancement in Dielectric and Magnetic Properties of $\text{Bi}_{1-x}\text{Ca}_x\text{FeO}_3$ ( $x = 0.2$ and $0.4$ ) Ceramics

Kuldeep Mehta<sup>1</sup> · Aditya Sharma<sup>1</sup> · Jaiparkash<sup>1</sup>

Received: 28 February 2022 / Accepted: 18 May 2022 / Published online: 10 June 2022  
© The Minerals, Metals & Materials Society 2022

## Abstract

In this study, to arrest the volatile Bi, a two-stage rapid solid-state reaction method has been adopted to prepare  $\text{Bi}_{1-x}\text{Ca}_x\text{FeO}_3$  ( $x = 0.2$  and  $0.4$ ) ceramics. Rietveld refinement on x-ray diffraction data confirmed the single-phase nature of the prepared samples. Unit cell volume of hexagonal structured (space group;  $R3c$ )  $\text{Bi}_{1-x}\text{Ca}_x\text{FeO}_3$  decreases with the increase of Ca concentrations. Temperature-dependent (250 K to 450 K) dielectric constant measurements have been performed at different frequencies (100 kHz, 300 kHz, 500 kHz, 700 kHz, 900 kHz and 1100 kHz). The dielectric constant ( $\epsilon'$ ), loss tangent ( $\tan \delta$ ) and ac-conductivity ( $\sigma_{ac}$ ) remain nearly constant for low temperatures ( $\sim 250$  K to  $\sim 365$  K) and have shown enhancement at higher temperatures (365 K to 450 K). Higher values of  $\epsilon'$ ,  $\tan \delta$  and  $\sigma_{ac}$  are detected in case of  $\text{Bi}_{0.6}\text{Ca}_{0.4}\text{FeO}_3$  sample. The butterfly-like loop in capacitance versus voltage curves confirms a weak ferroelectric nature. Magnetic field-dependent magnetization supports the Ca doping induced weak ferromagnetic character and exchange bias effect in the  $\text{Bi}_{0.6}\text{Ca}_{0.4}\text{FeO}_3$  sample. The origin of high dielectric constant and weak ferromagnetic nature is briefly discussed by considering the structural perturbations and cationic interaction in the  $\text{Bi}_{1-x}\text{Ca}_x\text{FeO}_3$  ( $x = 0.2$  and  $0.4$ ) ceramics.

**Keywords**  $\text{Bi}_{1-x}\text{Ca}_x\text{FeO}_3$  · XRD · dielectric · magnetization

## Introduction

Multiferroic materials are having applications in memory storage devices, multiple-state memories, and new data storage media.<sup>1–3</sup> Specifically, the multiferroics of  $\text{BiFeO}_3$ ,  $\text{BiMnO}_3$  and  $\text{YMnO}_3$  were found to have huge scope for research due to the simultaneous existence of ferroelectricity and magnetism.  $\text{BiFeO}_3$  (BFO) is one of the best multiferroic materials showing ferroelectricity and magnetism at room temperature (300K). It is a widely studied material owing to its relatively high Curie temperature ( $T_C = 1103$  K) and Neel temperature ( $T_N = 643$  K) with G-type antiferromagnetism.<sup>4,5</sup> The single-phase bulk  $\text{BiFeO}_3$  exhibits a rhombohedral distorted perovskite structure with space group  $R3c$ . All of the ions along the  $\{111\}_c$  direction are displaced relative to the ideal centrosymmetric positions, and

oxygen octahedra rotate alternately clockwise and counter-clockwise about the  $\{111\}_c$  direction. The off-centered distortion triggered by a stereochemically active  $\text{Bi}^{3+}$  lone pair gives rise to ferroelectric properties, whereas partially filled 3d orbitals of  $\text{Fe}^{3+}$  ions result in G-type antiferromagnetic ordering due to super-exchange interactions.<sup>6</sup> The antiferromagnetic characters and large leakage current are the major issues to the practical applications of BFO.<sup>7,8</sup> There are studies to overcome the antiferromagnetic characters and large leakage current of BFO by substituting  $\text{Bi}^{3+}$  with both trivalent rare-earth ions and divalent ions.<sup>2,9–12</sup> The enhanced magnetization due to structural distortion was observed in high pressure synthesized BFO ceramics.<sup>13</sup> Saturated ferroelectric and ferromagnetic hysteresis loops have been reported by substituting  $\text{Bi}^{3+}$  with  $\text{La}^{3+}$ ,  $\text{Nd}^{3+}$ ,  $\text{Sm}^{3+}$  and  $\text{Ba}^{2+}$  ions.<sup>11,12</sup> The partial substitution of  $\text{Bi}^{3+}$  with  $\text{La}^{3+}$  and  $\text{Fe}^{3+}$  with  $\text{Mn}^{4+}$  have improved magnetic properties.<sup>14</sup> Heterovalent doping up to 30% at Bi site in BFO has already been attempted by several researchers.<sup>15,16</sup> However, specific doping may enrich the multiferroic properties of BFO and remove the obstacles in its practical applications. Keeping this in mind,  $\text{Bi}_{1-x}\text{Ca}_x\text{FeO}_3$  ( $x = 0.2$  and  $0.4$ ) ceramics have

✉ Jaiparkash  
jaiparkash.manu@gmail.com

<sup>1</sup> Department of Physics, Manav Rachna University,  
Faridabad, Haryana, India

been synthesized using rapid two-stage solid-state reaction method, and their structural, dielectric, and magnetic properties are reported in this study.

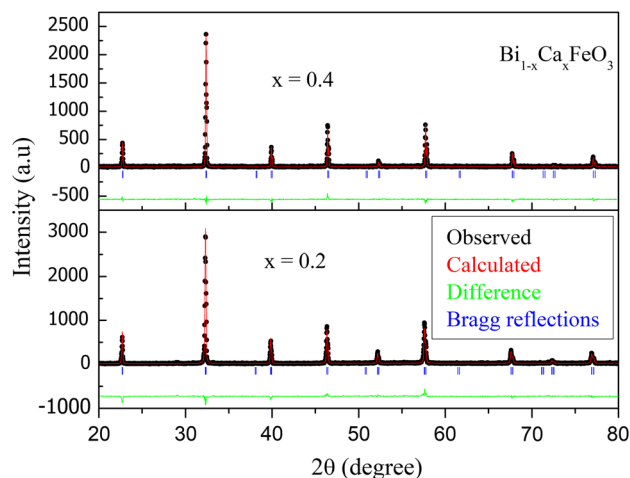
## Experimental Details

Using a rapid two-stage solid-state reaction method involving heating of the samples near the decomposition temperatures of the reagents, the bulk samples of  $\text{Bi}_{1-x}\text{Ca}_x\text{FeO}_3$  ( $x = 0.2$  and  $0.4$ ) were synthesized. This method was adopted to arrest the volatile Bi. For sample preparation, the pure form (99.99% pure, from Sigma Aldrich) of  $\text{Bi}_2\text{O}_3$ ,  $\text{Fe}_2\text{O}_3$  and  $\text{CaCO}_3$  were weighed in desired stoichiometric proportions and continuously ground for 2 h using agate mortar resulting in a fine, uniformly mixed powder. Later, the uniformly mixed powdered samples were pelletized using a pelletizer by applying a pressure of 2.5 t for 2 min. The pellets were heated from room temperature to  $850^\circ\text{C}$  with a uniform increment of  $2^\circ\text{C}$  per minute and dwelled at this temperature for 30 min in the first stage. The pellets were quenched by removing them from the furnace at the same temperature (i.e.  $850^\circ\text{C}$ ). Consequently, the pellets are again crushed and ground using pestle and mortar for 2 h and pelletized again. In the second stage, the heating was done for 10 min at  $900^\circ\text{C}$  and  $950^\circ\text{C}$  for  $x = 0.2$  and  $0.4$ , respectively. The samples were quenched by removing them from the furnace at given temperatures. X-ray diffraction (XRD) measurements were performed at room temperature using a Bruker-D8 x-ray diffractometer. *Cu K $\alpha$*  radiation with a wavelength of  $1.5418 \text{ \AA}$  was used with an operating voltage of 40 kV accelerating tube current of 40 mA. XRD data were collected within the two-theta range of  $20^\circ$ – $80^\circ$ . The scan speed was  $1^\circ/\text{min}$  with a step of  $0.02^\circ$ . The temperature and frequency-dependent dielectric measurements were performed using an Agilent precision LCR meter in the temperature range 250–450 K and frequency range 100–1100 kHz. The field-dependent magnetic measurement was performed at room temperature using a vibrating sample magnetometer (VSM).

## Results and Discussion

### Structural Study

Rietveld refinement, using FULLPROF code, was applied to the XRD data collected from  $\text{Bi}_{1-x}\text{Ca}_x\text{FeO}_3$  ( $x = 0.2$  and  $0.4$ ) samples. Figure 1a–b shows the XRD pattern along with the fitted curve and difference line. The agreement between observed and calculated data suggests that  $\text{Bi}_{1-x}\text{Ca}_x\text{FeO}_3$  samples are in a single phase for given concentration of Ca. The respective Wyckoff positions of Bi/

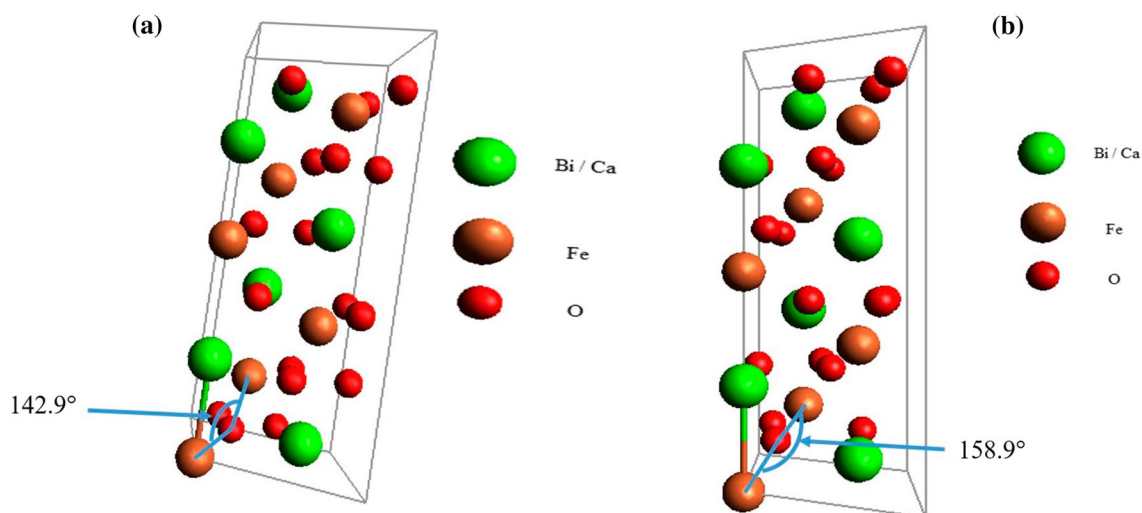


**Fig. 1** (a–b) X-ray diffraction pattern for  $\text{Bi}_{1-x}\text{Ca}_x\text{FeO}_3$  samples ( $x = 0.2$  and  $0.4$ ) measured at room temperature.

Ca, Fe and O are  $6a(0, 0, z)$ ,  $6a(0, 0, 0)$ , and  $18b(x, y, z)$  in  $\text{Bi}_{1-x}\text{Ca}_x\text{FeO}_3$  ( $x = 0.2, 0.4$ ). Table 1 depicts all the parameters related to the unit cell. It is evident from Table 1, that there is a decrease in the lattice parameters as well as the volume of the unit cell upon increasing the Ca doping concentration, which could be ascribed to either a smaller ionic radius of  $\text{Ca}^{2+}$  as compared to  $\text{Bi}^{3+}$  or to the formation of oxygen vacancies to neutralize/accommodate charge imbalance.<sup>17–19</sup> XRD pattern reveals that the Bragg reflections are sharp for both samples. No structural phase transition has been observed as mentioned in few publications on heterovalent doped  $\text{BiFeO}_3$ .<sup>20</sup> It can be noticed that with increasing the Ca doping from  $x = 0.2$  to  $x = 0.4$ , the intensity of the peaks is decreasing. This suggests a lattice distortion in the compound because of Ca doping and is analogous to a previous report.<sup>21</sup> Lattice strain has also been calculated using a Williamson–Hall plot (Refer to Table 1) and is found to increase with doping. It is also evidenced that the crystallite size is increasing ( $\sim 39 \text{ nm}$  to  $\sim 44 \text{ nm}$ ) with the increase in doping which reveals that substitution of  $\text{Bi}^{3+}$  with  $\text{Ca}^{2+}$  makes the crystal growth easy. This might be because volatile  $\text{Bi}^{3+}(\text{Bi}_2\text{O}_3)$  is being replaced by non-volatile  $\text{Ca}^{2+}(\text{CaCO}_3)$  resulting easy crystal growth.<sup>20</sup> The nano-range crystallite size may help in breaking the spiral spin structure and can reduce the leaky behavior of  $\text{BiFeO}_3$  system.<sup>22</sup> The Fe–O–Fe bond angle also shrinks with the increase of Ca doping which can alter the magnetic properties of the material. Figure 2a–b displays the crystal structure in hexagonal representation. Avogadro software has been used to generate this structure. The unit cell consists of six Bi/Ca, six Fe atoms and 18 oxygen atoms. The Fe–O–Fe bond angles have been shown to govern the magnetic properties.

**Table I** Lattice and refinement parameters for  $\text{Bi}_{1-x}\text{Ca}_x\text{FeO}_3$  ( $x = 0.2, 0.4$ )

Sample Name $\text{Bi}_{1-x}\text{Ca}_x\text{FeO}_3$	Lattice parameter (Å)	Wyckoff positions	Volume of the unit cell (Å <sup>3</sup> )	$\chi^2$ and R-factors	Average crystallite size (nm)	Strain	Fe-O-Fe bond angle (°)
$x = 0.2$	$a = 5.5401$ $c = 13.5617$	<b>Bi/Ca</b> <b>x y z</b> 0 0 0.22548 <b>Fe</b> 0 0 0 <b>O</b> 0.90443 0.74981 0.37984	360.48	1.44 $R_p = 24.6$ $R_{wp} = 26.2$ $R_{exp} = 21.79$	38.94	0.0015	142.9
$x = 0.4$	$a = 5.5282$ $c = 13.5424$	<b>Bi/Ca</b> <b>x y z</b> 0 0 0.24035 <b>Fe</b> 0 0 0 <b>O</b> 0.84038 0.62188 0.43483	358.42	1.33 $R_p = 34.8$ $R_{wp} = 32.9$ $R_{exp} = 28.48$	43.67	0.0020	158.9

**Fig. 2** (a–b) Crystal structure for  $\text{Bi}_{1-x}\text{Ca}_x\text{FeO}_3$  ( $x = 0.2, 0.4$ ) in hexagonal representation.

## Dielectric Study

Figure 3a–b shows the temperature-dependent dielectric constant ( $\epsilon'$ ) and Fig. 3c–d shows loss tangent ( $\tan\delta$ ) of  $\text{Bi}_{1-x}\text{Ca}_x\text{FeO}_3$  ( $x = 0.2$  and  $0.4$ ) samples at different applied frequencies. Both the samples show high value of dielectric constant and small value of loss tangent at room temperature. In Table II, the values of dielectric constant at room temperature, remanent magnetization and maximum value of magnetization of  $\text{Bi}_{0.6}\text{Ca}_{0.4}\text{FeO}_3$  along with recently reported multiferroics<sup>23,24</sup> have been presented. It is clear from the tabulated parameters that  $\text{Bi}_{0.6}\text{Ca}_{0.4}\text{FeO}_3$  depicts a very high value of dielectric constant in comparison to

other recently reported samples. The dielectric constant ( $\epsilon'$ ) and the loss tangent ( $\tan\delta$ ) remain nearly constant for both the samples at lower temperatures due to freezing of dipoles. At higher temperatures, both rise significantly along with temperature, which might be attributed to the distorted system caused by the formation of oxygen vacancies due to  $\text{Ca}^{2+}$  doping. Both  $\epsilon'$  and  $\tan\delta$  increase significantly in higher temperature regions. This increase may be attributed to the formation of dipoles created due to oxygen vacancies resulting in a distorted system. Therefore, the fundamental idea of band conduction might be supplanted by localized sites, which are surrounded by high potential wells that cannot be transcended/exceeded by electrons. The consequences

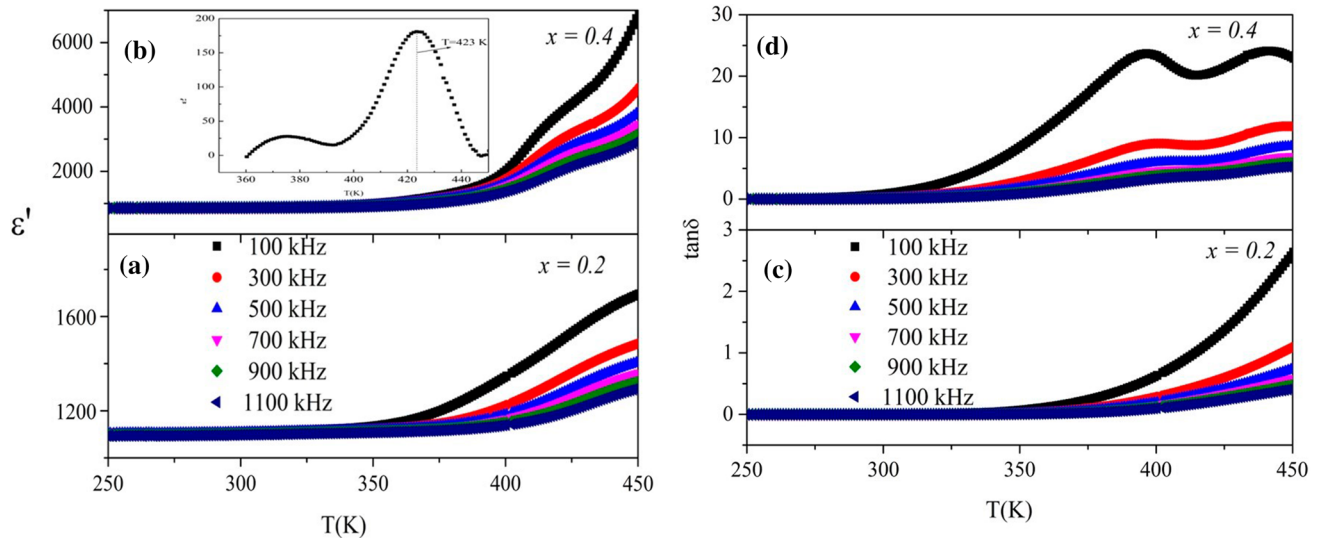


**Fig. 3** (a–b) Temperature dependence of dielectric constant ( $\epsilon'$ ) for  $\text{Bi}_{1-x}\text{Ca}_x\text{FeO}_3$  ( $x = 0.2, 0.4$ ). (c–d) Temperature dependence of loss tangent ( $\tan\delta$ ) for  $\text{Bi}_{1-x}\text{Ca}_x\text{FeO}_3$  ( $x = 0.2, 0.4$ ).

**Table II** Magnetic and dielectric data of recently reported multiferroics along with  $\text{Bi}_{0.6}\text{Ca}_{0.4}\text{FeO}_3$

Sample	$M_r$	$M_s$	$\epsilon'$ at 300 K & 100 kHz	Reference
$\text{YFeO}_3$	0.015	0.34	34	23
$\text{Y}_2\text{FeAlO}_6$	0.073	0.359	157	24
$\text{Bi}_{0.6}\text{Ca}_{0.4}\text{FeO}_3$	0.00035	0.00332	887	

of dipole creation at the localized hopping sites result in dielectric polarization. Thus, the phenomenon of localized charge between spatially fluctuating potentials may result in conduction as well as dipolar effects.<sup>16</sup>

Upon increasing the temperature, hopping of the charge increases, resulting in more conduction and dipolar effects which increases both dielectric constant and loss tangent. Hence, the rise in the value of both parameters on increasing temperature indicates that carrier hopping plays a major part at higher temperatures in both the samples.<sup>25</sup> The increase in loss tangent with temperature is a reflection of leakage current also which hinders its application for preparing storage devices. But a negligibly small value of loss tangent and hence leakage current at room temperature indicates a positive signal for its technological applications. However, at lower temperatures, hopping contributes a little to polarisation because of freezing of dipoles, resulting in insignificant variation in  $\epsilon'$  and  $\tan\delta$  with temperature. The variation is shown in the value of  $\epsilon'$  and  $\tan\delta$  with temperature and is obeyed at all frequencies in the measured frequency range (100–1100 kHz). Also, all these parameters decrease with an increase in

frequency, indicating that at low-frequency, dipoles created because of charge defects follow the field reversal bringing about the increased value of  $\epsilon'$  and  $\tan\delta$ . However, on increasing the frequency, the defect-related dipoles lag behind the field, and consequently the values of  $\epsilon'$  and  $\tan\delta$  decrease. It is evidenced that with increasing calcium doping concentration, the values of both  $\epsilon'$  and  $\tan\delta$  increase by almost threefold at 450 K. This may be due to the increased oxygen vacancies created because of Ca doping leading to hopping current and dipolar effects.<sup>26</sup> A dielectric abnormality has been noticed in the case of the  $\text{Bi}_{0.6}\text{Ca}_{0.4}\text{FeO}_3$  sample at 423 K in the  $\epsilon'$  versus temperature curve (see the inset of Fig. 3b), proposing some sort of ferroelectric transition, conceivably because of some structural transformation and ordering of dipoles. Because of the upper-temperature limit (450 K) of the instrument, we could not verify whether this anomaly is original or new. Further, more research is required to confirm the nature of the anomaly. Hence, to get a fine and clear view of observed peaks, the background has been subtracted for the  $\epsilon'$  vs. temperature curve at 100 kHz. It should also be noted that no such abnormality has been observed for the  $\text{Bi}_{0.8}\text{Ca}_{0.2}\text{FeO}_3$  sample up to 450K. For additional examination of the anomaly, variation in capacitance was recorded with respect to change in bias voltage at 420 K instead of ferroelectric hysteresis loops and is presented in Fig. 4. The butterfly-like loop in capacitance versus voltage curves are noticed which is an obvious sign of weak ferroelectric behavior in the samples.<sup>27</sup> Hence, we can conclude that the observed anomaly is due to certain ferroelectric transitions in the samples.

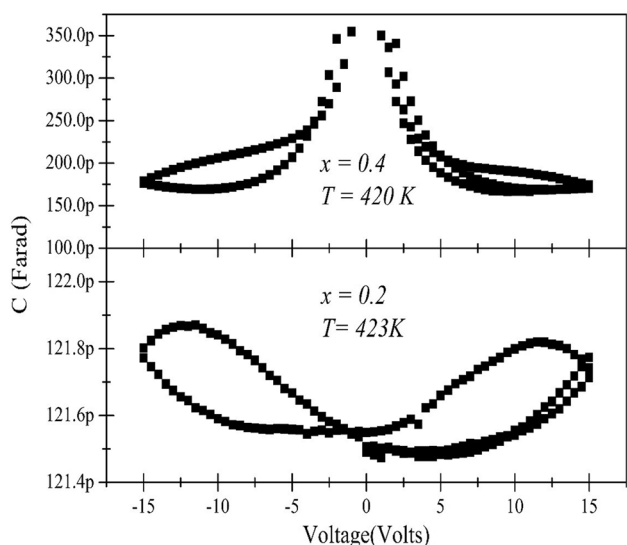


Fig. 4 Capacitance (C) versus voltage (V) curves  $\text{Bi}_{1-x}\text{Ca}_x\text{FeO}_3$  ( $x = 0.2, 0.4$ ) obtained at 1100 kHz.

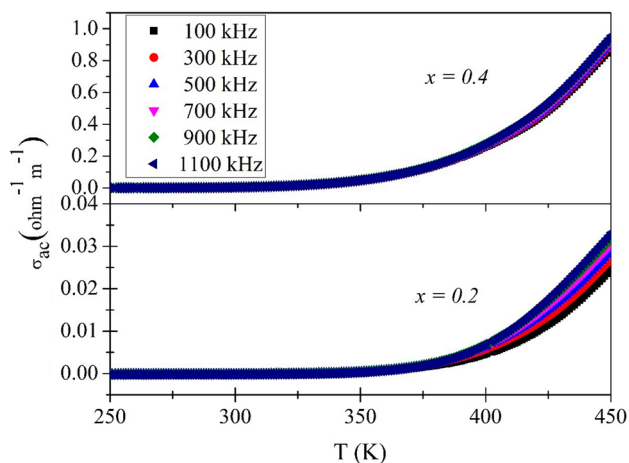


Fig. 5 Temperature dependence of ac-conductivity ( $\sigma_{ac}$ ) for  $\text{Bi}_{1-x}\text{Ca}_x\text{FeO}_3$  ( $x = 0.2, 0.4$ ).

**AC Conductivity Study**

Figure 5 displays the temperature dependence of ac-conductivity ( $\sigma_{ac}$ ) of  $\text{Bi}_{1-x}\text{Ca}_x\text{FeO}_3$  ( $x = 0.2, 0.4$ ) samples at selected frequencies. It is clear from the figure that conductivity increases exponentially with temperature obeying the Arrhenius equation  $\sigma_{ac} = \sigma_o e^{-E_a/kT}$ , where  $\sigma_o$  the pre-exponential constant and  $E_a$  is the activation energy. Also, the conductivity is increasing with the increase in frequency. This increase in the value of conductivity with an increase in temperature and frequency indicates that hopping has a significant role in both the samples.<sup>28</sup> The value of the activation energy for both the samples has been calculated (at

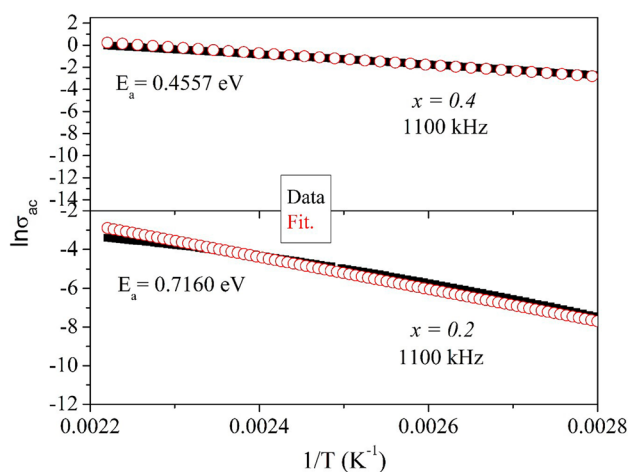


Fig. 6. Temperature dependence of  $\ln(\sigma_{ac})$  for  $\text{Bi}_{1-x}\text{Ca}_x\text{FeO}_3$  ( $x = 0.2, 0.4$ ) at 1100 kHz.

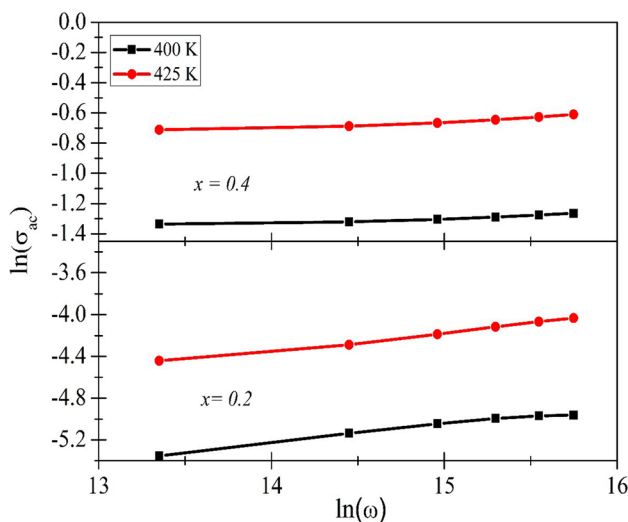
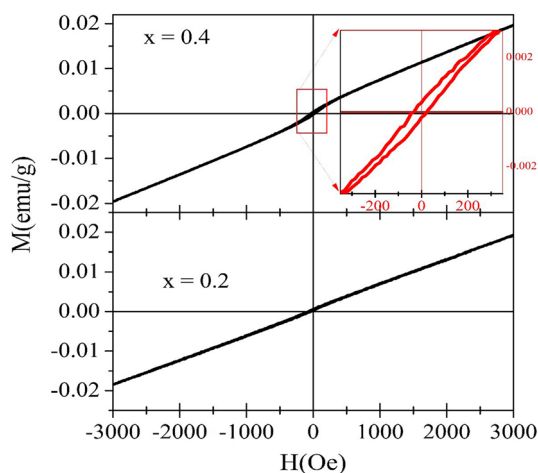


Fig. 7 Frequency dependence of  $\ln(\sigma_{ac})$  for  $\text{Bi}_{1-x}\text{Ca}_x\text{FeO}_3$  ( $x = 0.2, 0.4$ ) at 400 and 425 K.

1100 kHz) by finding the slope of graph  $\ln(\sigma_{ac})$  versus  $T^{-1}$  and results are presented in Fig. 6. The activation energy decreases while the conductivity increases as the doping is increased from 20% to 40% indicating that doping of calcium is making the conduction path easy, which might be due to an enhancement in oxygen vacancies with the increase in ca-doping. This indicates that small polaron hopping might be responsible for the  $\sigma_{ac}$ . To identify the hopping model,  $\ln(\sigma_{ac})$  has been plotted against  $\ln(\omega)$  at different temperatures for both the samples and presented in Fig. 7. The slopes have been found to increase with the increase in temperature which is the signature of small polaron hopping in both samples.<sup>29,30</sup> The figure of merit ( $F = \sigma_{ac}/\epsilon'$ ) which is related to the response time has also been calculated at selected

**Table III** Dielectric constant ( $\epsilon'$ ), conductivity ( $\sigma_{ac}$ ) and figure of merit (F) at selected frequencies at 400K

x	Frequency (kHz)	$\epsilon'$	$\sigma_{ac}$ ( $\Omega^{-1}\text{m}^{-1}$ )	F ( $\text{ohm}^{-1}\text{m}^{-1}$ )
0.2	100	1346.49	0.00473	$3.52 \times 10^{-6}$
	300	1224.12	0.00588	$4.80 \times 10^{-6}$
	500	1185	0.00643	$5.43 \times 10^{-6}$
	700	1164.27	0.00677	$5.81 \times 10^{-6}$
	900	1150.74	0.00694	$6.03 \times 10^{-6}$
	1100	1139.85	0.00701	$6.14 \times 10^{-6}$
0.4	100	2026.88	0.26276	$1.29 \times 10^{-4}$
	300	1769.55	0.26682	$1.50 \times 10^{-4}$
	500	1633.91	0.27114	$1.66 \times 10^{-4}$
	700	1553.61	0.27539	$1.79 \times 10^{-4}$
	900	1451.68	0.2792	$1.92 \times 10^{-4}$
	1100	1380.97	0.28254	$2.05 \times 10^{-4}$

**Fig. 8** Isothermal magnetization hysteresis for  $\text{Bi}_{1-x}\text{Ca}_x\text{FeO}_3$  ( $x = 0.2, 0.4$ ) at 300K.

frequencies and its value has been tabulated in Table III. It is clear from the Table III that the value of F increases approximately 100 times as the Ca doping is increased from 20% to 40%. The higher value of F suggests that the material is a potential candidate for solar cell applications.

### Magnetization Study

To understand the effect of Ca concentration on the magnetic properties of  $\text{BiFeO}_3$ , magnetic hysteresis loops have been measured over  $\pm 3000$  Oe at room temperature (300K) for both of the samples and are presented in Fig. 8. A small M-H loop specifically in the sample doped at 40% has been observed. Non-zero values of remanent magnetization ( $M_r$ ) and coercive field ( $H_c$ ) are also observed (see the inset of the upper panel). This proves that at room temperature, some

magnetic ordering exists in  $\text{Bi}_{0.6}\text{Ca}_{0.4}\text{FeO}_3$ . The magnetization does not saturate up to 3000 Oe magnetic field. The presence of remanent magnetization and coercivity indicates that the antiferromagnetic ordering of  $\text{BiFeO}_3$  is transformed to some ferromagnetic ordering or canted antiferromagnetic ordering. In a previous report, the stoichiometry of various ionic species in  $\text{BiFeO}_3$  was altered to balance the charge neutrality on Ca doping which may be due to the creation of O vacancies.<sup>17</sup> In the present case, due to the smaller radius of  $\text{Ca}^{2+}$  as compared to  $\text{Bi}^{3+}$ , the structure gets slightly strained as is clear from strain values calculated from x-ray diffraction data (refer to Table I). As a result, the Fe-O-Fe bond angle (Table I) changes and resulting in enhanced magnetic properties of the doped BFO. Also, the nano-dimensional crystallite size may also suppress the spiral spin structure giving rise to enhanced magnetic properties. The asymmetric behavior in the case of the sample doped at 40% in both directions indicates exchange bias in the system contrary to the Ba-doped sample.<sup>31</sup> The upgrading in the magnetic properties of  $\text{BiFeO}_3$  may be due the following three factors<sup>32</sup>: (i) suppression of the spiral spin structure due to small crystallite size, (ii) increase in spin canting due to the lattice strain, (iii) oxygen deficiency.<sup>31,32</sup> Oxygen vacancies created due to Ca doping may alter the antiferromagnetic interaction into ferromagnetic interaction, i.e. there may be statistical distribution of two types of magnetic interactions in the samples, which is confirmed by the asymmetric nature of the M- H loop (see Fig. 8).

### Conclusions

Single-phase polycrystalline  $\text{Bi}_{1-x}\text{Ca}_x\text{FeO}_3$  ( $x = 0.2$  and  $0.4$ ) samples have been prepared using a rapid two-stage solid-state reaction. The increase in the doping of Ca substitution in  $\text{BiFeO}_3$  (at Bi-site) does not change the parent crystal structure. However, both the lattice parameters 'a' and 'c' are found to decrease systematically with the incorporation of Ca. The  $\epsilon'$ ,  $\tan \delta$  and  $\sigma_{ac}$  were nearly invariant for the low-temperature regime ( $\sim 250$  K to  $\sim 365$  K). Further increase in the applied temperature up to 450 K leads to significant enhancement in  $\epsilon'$  and  $\tan \delta$  which is ascribed to the oxygen defect formation. Interestingly,  $\epsilon'$  is significantly increased for the sample containing a higher amount of Ca while the other parameters (i.e., applied temperature and frequency) were kept the same. An increase in  $\sigma_{ac}$  and a decrease in activation energy with an increase in Ca doping concentrations is the signature of small polaron hopping in the compound. The non-zero remanent magnetization and the existence of coercivity in the  $\text{Bi}_{0.6}\text{Ca}_{0.4}\text{FeO}_3$  sample indicate that the antiferromagnetic ordering of parent  $\text{BiFeO}_3$  is transformed to some ferromagnetic ordering.

**Acknowledgment** The authors are thankful to the honorable vice-chancellor and dean of Manav Rachna University, Faridabad, for constant encouragement and support for conducting research in the physics department.

**Conflict of interest** The authors declare that they have no conflict of interest.

## References

1. J.F. Scott, *Nat. Mater.* 6, 256 (2007).
2. S.T. Zhang, Y. Zhang, M.H. Lu, C.L. Du, Y.F. Chen, Z.G. Liu, Y.Y. Zhu, N.B. Ming, and X.Q. Pan, *Appl. Phys. Lett.* 88, 162901 (2006).
3. Y.H. Lee, J.M. Wu, and C.H. Lai, *Appl. Phys. Lett.* 88, 042903 (2006).
4. Z.X. Cheng, X.L. Wang, K. Ozawa, and H. Kimura, *Appl. Phys. Lett.* 88, 132909 (2006).
5. Z.X. Cheng and X.L. Wang, *Phys. Rev. B* 75, 172406 (2007).
6. G.L. Yuan, S.W. Or, Y.P. Wang, Z.G. Liu, and J.M. Liu, *Solid State Comm.* 76, 138 (2006).
7. A.K. Pradhan, K. Zhang, D. Hunter, J.B. Dadson, G.B. Loitts, P. Bhattacharya, R. Katiyar, J. Zhang, D.J. Sellmyer, U.N. Roy, Y. Cui, and A. Burger, *J. Appl. Phys.* 97, 093903 (2005).
8. M.M. Kumar and V.R. Palkar, *Appl. Phys. Lett.* 76, 2764 (2000).
9. Y.H. Lin, Q. Jiang, Y. Wang, C.W. Nan, L. Chen, and J. Yu, *Appl. Phys. Lett.* 90, 172507 (2007).
10. D. Lee, M.G. Kim, S. Ryu, H.M. Jang, and S.G. Lee, *Appl. Phys. Lett.* 86, 222903 (2005).
11. G.L. Yuan and S.W. Or, *J. Appl. Phys.* 100, 024109 (2006).
12. D.H. Wang, W.C. Goh, M. Ning, and C.K. Ong, *Appl. Phys. Lett.* 88, 212907 (2006).
13. W.N. Su, D.H. Wang, Q.Q. Cao, Z.D. Han, J. Yin, J.R. Zhang, and Y.W. Du, *Appl. Phys. Lett.* 91, 092905 (2007).
14. V.R. Palkar, D.C. Kundaliya, and S.K. Malik, *J. Appl. Phys.* 93, 4337 (2003).
15. V.A. Khomchenko, D.A. Kiselev, J.M. Vieira, A.L. Kholkin, M.A. Sa, and Y.G. Pogorelov, *Appl. Phys. Lett.* 90, 242901 (2007).
16. V.A. Khomchenko, D.A. Kiselev, J.M. Vieira, L. Jian, A.L. Kholkin, A.M.L. Lopes, Y.G. Pogorelov, J.P. Araujo, and M. Maglione, *J. Appl. Phys.* 103, 024105 (2008).
17. V.A. Khomchenko, M. Kopcewicz, A.M.L. Lopes, Y.G. Pogorelov, J.P. Araujo, J.M. Vieira, and A.L. Kholkin, *J. Phys. D: Appl. Phys.* 41, 102003 (2008).
18. D. Kothari, V.R. Reddy, A. Gupta, V. Sathe, A. Banerjee, S.M. Gupta, and A.M. Awaasthi, *Appl. Phys. Lett.* 91, 202505 (2007).
19. B. Yu, M. Li, J. Liu, D. Guo, L. Pei, and X. Zhao, *J. Phys. D: Appl. Phys.* 41, 065003 (2008).
20. J. Li, Y. Duan, H. He, and D. Song, *J. Alloys and Compounds* 315, 259 (2001).
21. K.S. Rao, D.M. Prasad, P. Murali Krishna, B.H. Bindu, and K. Suneetha, *J. Mater. Sci.* 42, 7363 (2007).
22. A.R. Makhdoom, M.J. Akhtar, M.A. Rafiq, and M.M. Hassan, *Ceram. Int.* 38, 3829 (2012).
23. F.S. Jesus, C.A. Escobedo, and A.M.B. Miro, *Ceram. Int.* 44, 15298 (2018).
24. B. Song, J. Shen, H. Zhao, A. Kumar, Q. Xu, Y. Zhai, and Q. Li, *Ceram. Int.* 47, 10873 (2021).
25. N.R.M. Reddy, M.V. Ramana, K. Krishnaveni, K.V.S. Kumar, and V.R.K. Murthy, *Bull. Mater. Sci.* 30, 357 (2007).
26. Z. Yu, C. Ang, R. Guo, A.S. Bhalla, and L.E. Cross, *Appl. Phys. Lett.* 80, 1034 (2002).
27. N. Uchida and T. Ikeda, *Jpn. J. Appl. Phys.* 4, 867 (1965).
28. H. Bouaamlat, N. Hadi, N. Belghiti, H. Sadki, M.N. Bennani, F. Abdi, T. Lamcharfi, M. Bouachrine, and M. Abarkan, *Adv. Mater. Sci. Eng. Vol.* 8689150, 8 (2020).
29. N.F. Mott, *Philos. Mag.* 19, 835 (1969).
30. M.B. Bellakki and V. Manivannan, *J. Mater. Sci.* 45, 1137 (2010).
31. J. Nogues and I.K. Schuller, *J. Magn. Magn. Mater.* 192, 203 (1999).
32. R. Mazumder, P.S. Devi, D. Bhattacharya, P. Choudhury, A. Sen, and M. Raja, *Appl. Phys. Lett.* 91, 062510 (2007).

**Publisher's Note** Springer Nature remains neutral with regard to jurisdictional claims in published maps and institutional affiliations.